The Thermal Behavior of a Dual-Function Solar Collector Integrated with Building: An Experimental and Numerical Study on the Air Heating Mode

Jinwei Ma [1,*] **, Qiang Zhao** [1]**, Yuehong Su** [2]**, Jie Ji** [3]**, Wei He** [4]**, Zhongting Hu** [4]**, Tingyong Fang** [5] **and Haitao Wang** [5]

[1] School of Environment and Energy Engineering, Anhui Jianzhu University, Hefei 230601, China; zhaoqiang@ahjzu.edu.cn
[2] Department of Architecture and Built Environment, University of Nottingham, Nottingham NG7 2RD, UK; Yuehong.Su@nottingham.ac.uk
[3] Department of Thermal Science and Energy Engineering, University of Science and Technology of China, Hefei 230026, China; jijie@ustc.edu.cn
[4] Department of Building Environment and Equipment, Hefei University of Technology, Hefei 230009, China; Hwei@hfut.edu.cn (W.H.); hztwy@hfut.edu.cn (Z.H.)
[5] Anhui Province Key Laboratory of Intelligent Building & Building Energy Saving, Hefei 230601, China; ftyong@ahjzu.edu.cn (T.F.); wht@ahjzu.edu.cn (H.W.)
*   Correspondence: majw@mail.ustc.edu.cn; Tel.: +86-551-638-28-252

Abstract: This paper presented a novel solar collector that can work in air or water heating mode depending on the seasonal requirement. The dual-function solar collector (DFSC) integrated with a building as well as a reference building without the DFSC were built to test thermal behavior in passive air heating mode during winter. The buildings were equipped with an apparatus to control the room temperature. During the testing procedure, experimental study on the DFSC system was carried out under two conditions, where the indoor temperature was controlled and non-controlled. The results showed that the average temperature of the test room was about 3.43 °C higher than that of the reference room under the non-controlled condition. When the room temperature was controlled at 18 °C, the power consumptions of the test room and reference room were 4.322 kWh and 7.796 kWh, respectively. Consequently, the corresponding daily power consumption saved could reach up to around 3.5 kWh. Moreover, a dynamic numerical model on the DFSC along with the building was developed taking the fin effect of the Cu-tubes into account. The numerical results are found to be well consistent with the measured data. A parametric study on with/without Cu-tubes and depth of the air channel was carried out. It is found that the existing Cu-tubes functioning as water heating can enhance the air heating efficiency when the depth of air channel is of a suitable size.

Keywords: flat plate solar collector; dual-function; passive air heating; numerical modeling

1. Introduction

The utilization of renewable sources such as solar energy for building heating is an effective method to lower electricity consumption [1]. Trombe wall, which is known as one of the easiest and cheapest architectural devices to utilize solar energy, has been widely used [2,3]. The performance of Trombe wall has been analyzed. Bojic et al. [4] studied the use of a Trombe wall in Lyon-France and proved that it can reduce the yearly heating consumption by up to 20%.

Many scholars have modified the traditional Trombe wall in order to improve their efficiency. Different configurations have been developed, such as the Trombe–Michel wall [5], the Barra-Costantini

wall [6], and the PV-Trombe wall [7]. There are various components to help improve the efficiency, such as glazing, insulation, shading devices, vents, wall's materials and thicknesses, and air channel depth. Bellos et al. [8] proposed a Trombe wall with extra glazing in the massive wall, and it was compared with the classic Trombe wall and the insulated wall. Results showed that the indoor temperature was higher compared to the conventional cases and the lighting of the internal space was improved. Briga-Sá et al. [9] studied the non-ventilated and ventilated Trombe wall with various thickness in the storage wall. Results showed that energy heating needs can be reduced by 16.36% if a Trombe wall is added to the building envelope. Mootz and Bezian [10] set up the theoretical model of Trombe wall to analyze the influence of air channel depth on performance. Result indicated that there was a slight rise of efficiency when the channel depth exceeded 20 mm, and a channel depth between 15 and 20 mm was recommended. Burek and Habeb [11] conducted an experimental study on the mass flow rate and heat transfer in the Trombe wall. Results showed that the mass flow rate increases with the increasing heat input and air channel depth.

The application of Trombe wall can reduce energy consumption for space heating in winter, but it is problematic in temperate climates due to undesired heat gains and overheating phenomena in summer [12]. To extend the use of the passive heating system beyond the heating season and solve the overheating problem, some strategies have been proposed. Solar shading and activating ventilation were regarded as useful techniques to address these unfavorable problems [13].

Rockendorf et al. [14] designed a hybrid wall which has pipes attached to the surface, so that fluid could flow through the pipe system and cool the absorber. Results showed that more than 75% of the absorbed heat could be removed by the fluid and effective cooling was achieved. Based on this idea, a dual-function solar collector (DFSC) integrated with building was developed. Ji et al. [15,16] presented an experimental analysis on the performance, concluding that the indoor temperature was increased by 20 °C in winter, and the water heating efficiency was 37% in the non-heating season. In addition, the cooling load of the building could be reduced effectively in summer. Sergio L et al. [17] designed an air/water heating system that contained an air-to-water heat exchanger with the aim of alternative summer use, and hot air provided by the solar air heater was used for water heating while operating in summer conditions.

In the previous studies [16], DFSC was integrated with hotbox, the envelop of which are a lightweight insulation with a weak heat capacity, so there was a large temperature fluctuation within a day: The maximum room temperature was up to 29.8 °C and the minimum temperature was only about 0.5 °C; the temperature fluctuation was nearly 30 °C. In this paper, DFSC was integrated with a building, and the thermal characteristic in passive air heating mode was studied via both experimental and numerical approaches. Additionally, a reference room without the DFSC was also built. The innovations of the present work are as following: (i) Southern façade of the test building was made of bricks with high heat capacity, so the experiment can more accurately reflect the practical operation than the previous research. (ii) Comparative experiments were carried out in two conditions: Controlled indoor temperature and non-controlled indoor temperature. Indoor temperature was controlled so the effect of DFSC on building heating load can be directly obtained. (iii) Cu-tubes welded to the absorber plate would affect the heat transfer between the absorber and air flow. This factor has been taken into account when the theoretical model was established. (iv) The theoretical model was validated by the experiment and the impact of flow channel structure was investigated.

2. Experiment Setup

2.1. Description of the DFSC

The structure of the dual-function collector is shown in Figure 1. The collector has a length of 200 cm, a width of 100 cm and a thickness of 10 cm. The solid lateral surface of the DFSC channel and back sheet are well insulated from outside. The upper surface of the collector module covers a 3.2 mm-thick flat glass. The aluminum absorber is situated between the glazing cover and back sheet,

and its front surface is coated with selective material to maximize the absorption of the incident solar radiation. Cu-tubes welded on the rear surface of the absorber form the water flow channel in water heating mode. The absorber plate divides the air interlayer between the glass cover and the backboard of the module into the upper and lower parts: The cavity between the absorber plate and the bottom floor is the air flow channel in passive air heating mode. The up cavity between the absorber plate and glass cover can reduce the heat loss. The backboard is composed of 2 cm glass fiber along with iron plates for both inside and outside of the channel sides. Two opening vents with the dimension of 36 cm × 12 cm are positioned at the top and bottom of the blackboard of the module for the air heating mode of the DFSC. The parameters characteristic of the collector are listed in Table 1.
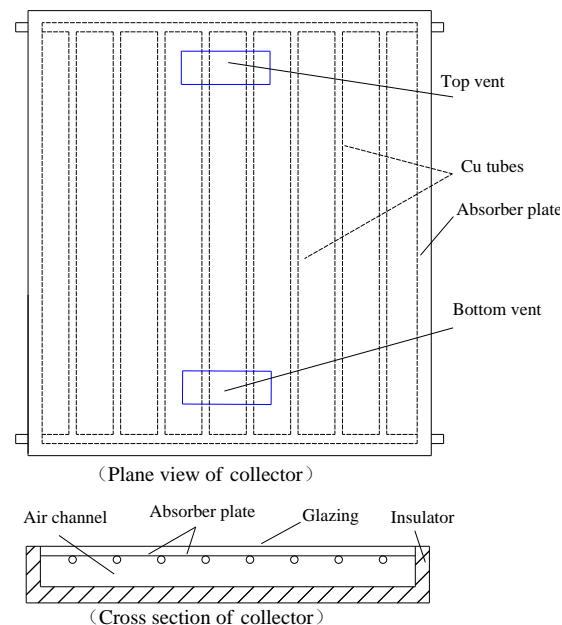
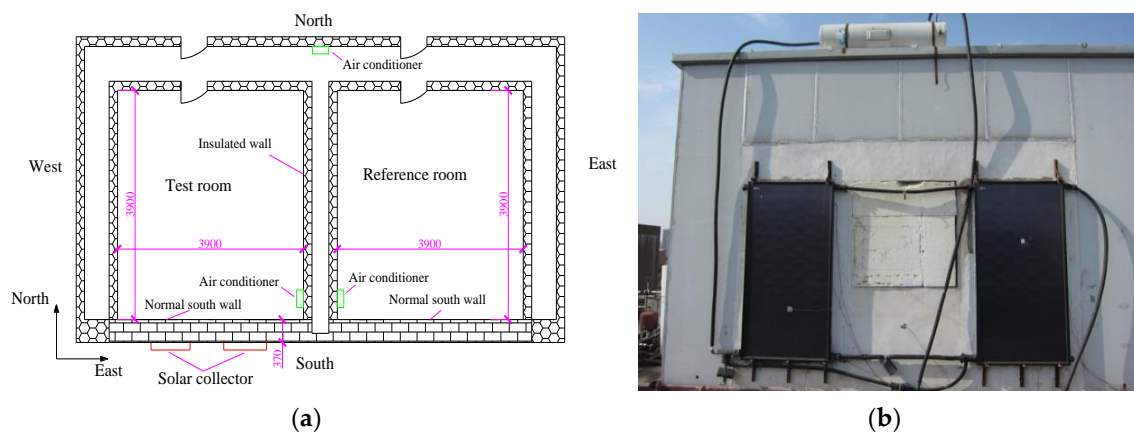**Figure 1.** Schematic diagram of the dual-function solar collector.

Table 1. Parameters characteristic of the collector.

Materials	Density (kg/m^3)	Specific Heat (J/kg K)	Thermal Conductivity (W/m K)	Absorptivity	Emissivity	Thickness (mm)
Glazing [1]	2500	750	1.05	0.038	0.83	3.2
Absorber	2720	933	237	0.9	0.05	0.4
Insulation	15	1210	0.04	-	-	20
Cu-tubes	8933	397	393	-	-	0.8

[1] Transmittance of the glazing is 0.912.

2.2. Experimental System

A hot box was built on the roof of an office building located in Hefei (31.89° N and 117.3° E), China. The experimental platform consists of two separate rooms with the same structure and dimensions. As shown in Figure 2a, the left room was equipped with two DFSCs called test room and the right one is the reference room. The dimensions of each room are 3.9 m (Width) × 3.9 m (Length) × 2.6 m (Height). The southern wall was constructed with bricks and all the other exterior walls and partitions of the hot box are made of insulation material sandwiched in metal plates. The appearance of the system is shown in Figure 2b. The thermal properties are listed in Table 2. In general, the experimental system can work in two different modes: Passive space heating in winter and water heating in other seasons. In this paper, we focus on the thermal behavior on the passive heating mode.

Figure 2. Views of the experimental system: (**a**) The horizontal cross-section schematic; (**b**) outside view showing the test room building.

Table 2. Parameters characteristic of the building envelop.

Materials	Density (kg/m^3)	Specific Heat (J/kg K)	Thermal Conductivity (W/m K)	Absorptivity	Emissivity	Thickness (mm)
Brick (SW)	1920	835	0.72	0.5	0.9	370
Steel panel	8030	502	16.27	0.5	0.9	0.5
Polystyrene	15	1500	0.04	-	-	300 (F)/50 (W)

SW—south wall; F—floor; W—other walls.

The cross-section view of the test room is shown in Figure 3. Modules were combined with the southern wall and the upper and lower vents connected the air channel and the indoor space for air circulation. The air vents would be opened at 8:00 when the heat could be delivered into the room through the passive circulation and closed at 17:00 to prevent heat loss from the room. The passive heating experiments were carried out in good weather conditions on 18–19 January and 3 March. The temperature measurement points include the absorber plate of DFSC, lower vent (air inlet), upper vent (air outlet), and the inner surface of the wall. In order to obtain the indoor temperature distribution, temperature sensors were arranged at three positions from top to bottom in the indoor centerline both in the test room and the reference room. Temperatures of building envelop, indoor air and components of the collector are important for the thermal behavior investigation of the system. In addition, they could be used for model validation. Figure 3 shows the positions of sensors. Temperatures were measured by the T-type thermocouples with an accuracy of ± 0.5 °C. The solar radiation received by the south wall facade was monitored by pyranometer (model TBQ-2, ± 11.104 µv/W m^{-2} and ± 11.601 µv/W m^{-2}). The horizontal wind speed was captured by the anemometer (model EC21A). Both the test room and reference room were equipped with a temperature control system so that the room temperature can be controlled to a fixed value. The electric consumption of the temperature control system was recorded. All the measured values were recorded by the data acquisition unit (Agilent model HP34970A) at an interval of 30 s.
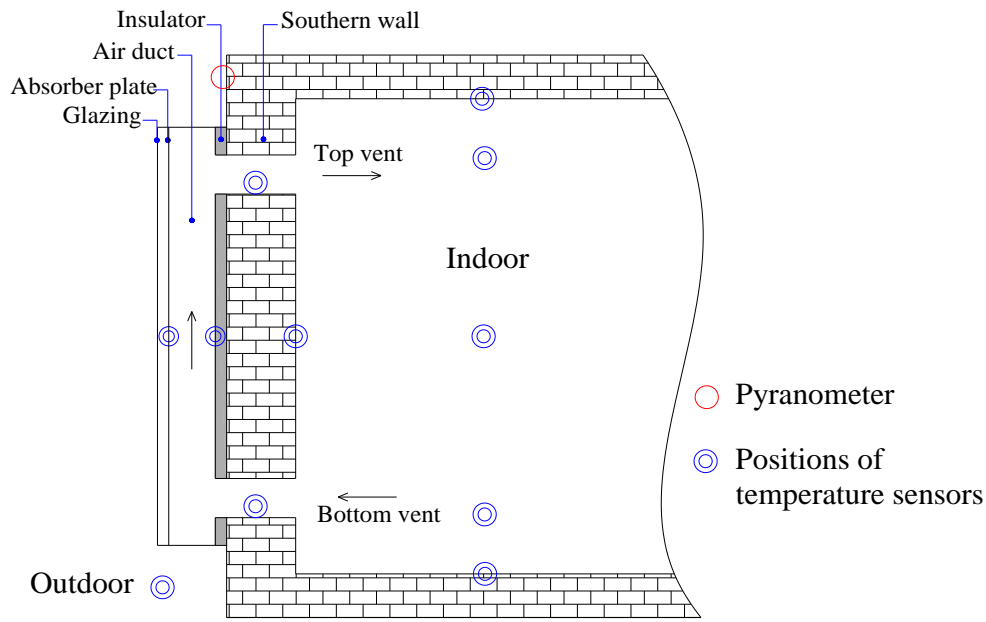
Figure 3. The schematic of test room with DFSC.

3. Numerical Modelling

The numerical model for passive air heating mode of the building with DFSC module was established. The model comprises three coupled parts: The DFSC model, the building envelops model, and the indoor air model by considering the solar radiation irradiated in the collector and absorbed by the absorber plate, convective heat transfer between the cavity air and the absorber plate, heat conduction through the backboard of DFSC and the wall, flow and heat transfer of the indoor air.

3.1. Modeling of DFSC

The essential components of the collector are the glass cover, the backboard, and the absorber plate. The air is heated by flowing in the channel through the buoyancy effect, the temperature difference in width direction could be neglected. On the other hand, the temperature distribution along the thickness direction can be neglected because of the miniature thickness of plate. Under the assumption that the temperatures of the glass cover, absorber, and the back plate vary only in the direction of air flow, the dynamic energy balance equations were established. The temperatures of the air stream and essential components can be obtained by solving the energy equations.

3.1.1. Governing Equations

The energy equation of the glass cover is one dimensional in the length direction:

$$\rho_g c_g d_g \frac{\partial T_g}{\partial t} = k_g d_g \frac{\partial^2 T_g}{\partial z^2} + hc_{pg}(T_p - T_g) + hr_{pg}(T_p - T_g) + hc_a(T_a - T_g) + hr_s(T_s - T_g) + \alpha_g S \quad (1)$$

The energy equation of the absorber plate is one dimensional in the length direction:

$$\rho_p c_p d_p \frac{\partial T_p}{\partial t} = k_p d_p \frac{\partial^2 T_p}{\partial z^2} - (hc_{pg} + hr_{pg})(T_p - T_g) - hr_{pb}(T_p - T_b) - hc_{pf}(T_p - T_f) + \alpha_p \tau_g S \quad (2)$$

Equation of the air stream in air channel of DFSC is given as

$$\rho_f c_f d \frac{\partial T_f}{\partial t} = \rho_f c_f u d \frac{dT_f}{dz} + hc_{pf}(T_p - T_f) + hc_{bf}(T_b - T_f) \quad (3)$$

where d is the depth of the air channel (distance between absorber plate and backboard), hc_{pf} is the convective heat transfer coefficient between the air flow and absorber plate, u is the speed of air flow. The DFSC has a similar construction to the conventional passive air collector except the absorber plate is partially welded with Cu-tubes as shown in Figure 1. The additional tubes can affect heat transfer between the absorb plate and the air stream. Moreover, the tubes affect the speed of air flow by changing the cross-sectional area of air channel. Taking the tubes into account, the calculation method of hc_{pf} and u is described in Section 3.1.2.

The energy equation of the interior plate of backboard is given as

$$\rho_b c_b d_b \frac{\partial T_b}{\partial t} = k_b d_b \frac{\partial^2 T_b}{\partial z^2} + hc_{bf}(T_f - T_b) + hr_{pb}(T_p - T_b) + \frac{k_R}{d_R}(T_{w,1} - T_b) \tag{4}$$

where d_R is the thickness of the insulation layer of backboard, and $T_{w,1}$ is the temperature of the outermost node of the southern wall that is attached with the backboard of DFSC.

3.1.2. Relative Heat Transfer Coefficient

The convective heat transfer coefficient in the air channel can be calculated by introducing the Nusselt number as

$$hc = \frac{\text{Nu}k}{d} \tag{5}$$

where d means the depth of the air channel (the interval between two planes). The Nusselt number for the air channel is calculated by Reference [18]:

$$Nu = \max\left\{1, 0.288\left(\frac{Ra}{K_A}\right)^{0.25}, 0.039Ra^{0.33}\right\} \text{ for the case in which air vents were closed} \tag{6}$$

$$Nu = 0.107Gr^{1/3} \text{ for the case in which air vents were open} \tag{7}$$

where the aspect factor $K_A = L/d$ (ratio between the length and the depth), $Ra = Gr \cdot \text{Pr}$, and Gr is Grashof number which is calculated by Reference [18]

$$Gr = \frac{\beta g L^3 (T_{sur} - T_f)}{\nu^2} \tag{8}$$

where T_{sur} is the temperature of absorber plate or the interior plate of the backboard.

Based on the Equation (5), the convective heat transfer coefficients between air stream and the interior plate of backboard can be calculated directly. However, there are several Cu-tubes welded on back side of the absorber plate, so the surface exposed to the air flow channel is not flat. Heat exchange between air stream, absorber plate and Cu-tubes is shown in Figure 4. The convective heat transfer coefficient between the air stream and absorber plate is different from the traditional flat plate without tubes. In air heating mode, the inner water channel composed by the Cu-pipe is closed and there is no water but air inside the pipes. The Cu-tubes can be seen as fins that increase the heat transfer area.
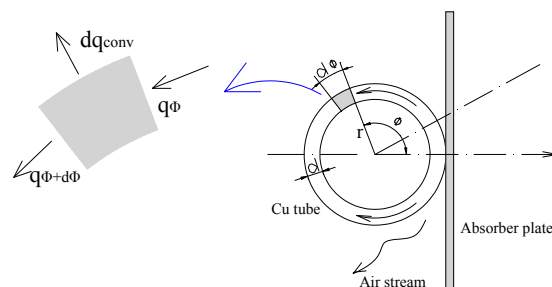

Figure 4. The schematic of the absorber plate welded with Cu-tubes.

As shown in Figure 4, for the differential element of the tube, the energy balance equation can be obtained that

$$q_\phi = q_{\phi+d\phi} + dq_{conv} \tag{9}$$

Based on Fourier law, it is known that

$$q_\phi = -\frac{k}{r} A_{t,C} \frac{dT}{d\phi} \tag{10}$$

where $A_{t,C}$ is the cross-section area. The conduction heat rate at $\phi + d\phi$ can be expressed as

$$q_{\phi+d\phi} = q_\phi + \frac{dq_\phi}{d\phi} d\phi = -\frac{k}{r} A_{t,C} \frac{dT}{d\phi} - \frac{k}{r} A_{t,C} \frac{d^2T}{d\phi^2} d\phi \tag{11}$$

The convection heat transfer is calculated by

$$dq_{conv} = hdA_S(T - T_\infty) \tag{12}$$

We can obtain that

$$\frac{hr^2}{kd}(T - T_\infty) - \frac{d^2T}{d\phi^2} = 0 \tag{13}$$

To simplify the form of equation, several parameters are defined as: $m^2 = \frac{h}{kd}$, $\alpha = r\phi$, $\theta(\alpha) = T(\alpha) - T_\infty$, then we can obtain

$$\frac{d^2\theta}{d\alpha^2} - m^2\theta(\alpha) = 0 \tag{14}$$

$$\theta(\alpha) = C_1 e^{m\alpha} + C_2 e^{-m\alpha} \tag{15}$$

To evaluate the C_1 and C_2, it is necessary to specify appropriate boundary conditions which are described as

$$\theta(0) = C_1 + C_2 = T_b - T_f = \theta(b) \tag{16}$$

$$\frac{d\theta}{d\alpha}\Big|_{\alpha=\pi} = C_1 e^{m\pi} - C_2 e^{-m\pi} = 0 \tag{17}$$

It can be obtained that

$$\frac{\theta}{\theta_b} = \frac{\cosh m(\pi r - \alpha)}{\cosh mr\pi} \tag{18}$$

Fin efficiency can be defined as [19]

$$\eta_{fin} = \frac{q_{fin}}{q_{\max}} \tag{19}$$

where

$$q_{fin} = -2kA_{t,C} \frac{d\theta}{d\alpha}\Big|_{\alpha=0} = 2kdm\theta_b \tanh mr\pi \tag{20}$$

and

$$q_{\max} = hA_s\theta_b = 2h\pi r\theta_b \tag{21}$$

where A_s is the exposed area that contains the tubes and plate. Then the convection coefficient can be calculated by

$$hc_{pf2} = hc \cdot (N\eta_{fin}P_t + w_p)/w_p \tag{22}$$

where hc is the convection coefficient for un-finned flat surface.

The air flow in the channel of DFSC is driven by the stack pressure, and the velocity can be calculated by [7]

$$u = \sqrt{\frac{0.5g\beta(T_{out} - T_{\text{in}})L}{\xi_{in}\left(\frac{A_{airc}}{A_{\text{in}}}\right)^2 + \lambda_f \frac{L}{D_e} + \xi_{out}\left(\frac{A_{airc}}{A_{out}}\right)^2}} \tag{23}$$

where λ_f is the friction loss coefficient of the channel, ξ_{in} and ξ_{out} are the partial resistance loss coefficients of the inlet vent and outlet vent, respectively. $\xi_{in} = 1.0$, $\xi_{out} = 1.5$. De is the hydraulic diameter of the air channel (m); Aairc is the cross section of air channel (m^2); Aout, Ain are the areas of the outlet and inlet vent, respectively (m^2); λ_f could be calculated by [7]

$$\lambda_f = 0.316\text{Re}^{-0.25} \qquad \text{for turbulent flow,} \tag{24}$$

$$\lambda_f = \frac{96}{\text{Re}}(1 - 1.20244\chi + 0.88119\chi^2 + 0.88819\chi^3 - 1.69812\chi^4 + 0.72366\chi^5) \text{ for laminar flow,} \tag{25}$$

where χ is the ratio of the depth and width of the air channel.

The calculation method of the convective heat transfer coefficient on exterior surface of the collector and the natural convective heat transfer coefficient in the air layer between the glass cover and absorber plate are the same as reference [15].

3.2. Modeling of Building

The essential components of the building envelope are the walls. The heat flux through walls of the building envelope is determined by one-dimensional along its thickness, so the energy balance equation of the wall is given as

$$\rho_w c_w \frac{\partial T_w}{\partial t} = k_w \frac{\partial^2 T_w}{\partial x^2} \tag{26}$$

Equation (24) is for ceiling, floor and four directions of the walls. The boundary conditions of the envelope are the energy balance on the surface, which is between the heat conducting from the surface to the inside of the wall and the heat transferring from surface to its ambient. The boundary condition at the exterior wall surface is

$$-k_w \frac{\partial T_w}{\partial x}\Big|_{x=0} = hc_a(T_w - T_a) + hr_a(T_w - T_s) \tag{27}$$

The southern wall is divided into two parts: The parts of exterior wall surface covered by DFSC and the remaining exposed parts. The parts covered by DFSC can be calculated coupled with the backboard of DFSC. For the south façade that remains exposed

$$-k_w \frac{\partial T_w}{\partial x}\Big|_{x=0} = hc_a(T_w - T_a) + hr_a(T_w - T_s) + \alpha_w S \tag{28}$$

The boundary condition at the interior surface of the envelop is

$$-k_w \frac{\partial T_w}{\partial x}\Big|_{x=Dw} = hc(T_w - T_{room}) \tag{29}$$

The convective heat transfer coefficient on inner surface of the walls is calculated by [20]

$$hc = 2.03\Delta T^{0.14} \tag{30}$$

The convective coefficient on the ceiling is expressed as [20]

$$hc = -0.166 + 0.484ACR^{0.8} \tag{31}$$

where ACH is the air exchange rate.

3.3. Modeling of Indoor Air

The heat balance equation for the room air needs to be discussed in two conditions: The vents are open or closed. When the upper and lower vents of the system are closed, the whole room can be seen as a node. The energy equation of the indoor air is expressed as

$$\rho_f V_{room} C_f \frac{dT_{room}}{dt} = \sum hc_{w,\,i} A_{w,i}(T_i - T_{room}) \tag{32}$$

When the vents are opened, the heat exchange caused by the air flowed from the channel of DFSC into the room should be considered. In this situation, the energy equation of the indoor air is given as

$$\rho_f V_{room} C_f \frac{dT_{room}}{dt} = \sum hc_{w,i} A_i(T_{w,i} - T_{room}) + \rho_f u A_{airc}(T_{out} - T_{room}) \tag{33}$$

3.4. Numerical Approaches

As a result of the finite difference method, the energy equations were transformed into algebraic equations, which were solved by the iteration method. In the solution procedure, the initial conditions including temperatures of different walls and operative environmental parameters such as solar radiation, the temperatures of indoor and outdoor were given based on the experimental data. In this study, numerical simulation under unsteady state was run with FORTRAN.

Temperatures of indoor temperature, envelops of building, air outlet, components of DFSC and the mass flow rate of air can be obtained by the numerical simulation. So, the efficiency of DFSC could be calculated by

$$\eta_a = \dot{m} C_p (T_{out} - T_{in})/(S A_c) \tag{34}$$

4. Results and Discussion

4.1. Model Validation

To validate the developed model, an experiment of the DFSC system was carried out from 18–19 January under the condition of non-controlled indoor temperature. During the whole test procedure, the air vents remained open from 8:00 to 17:00 and the water valves were closed. The experimental parameters including the vertical solar radiation and the temperatures of outside ambient are shown in Figure 5.
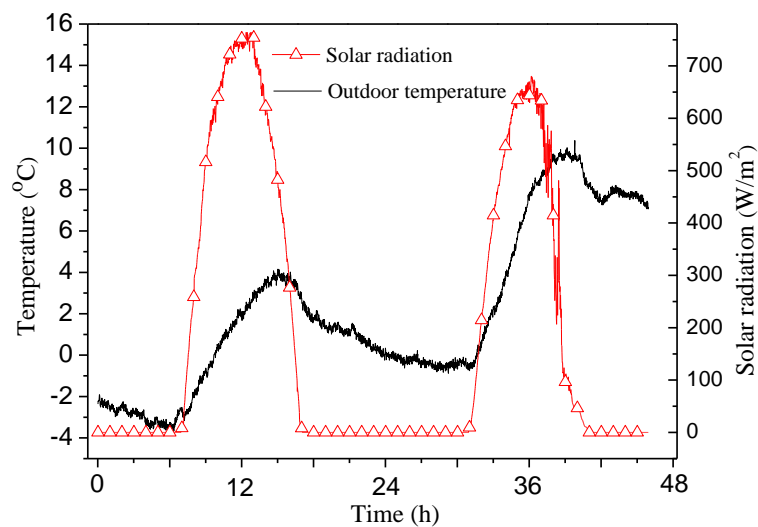

Figure 5. Solar radiation intensity and outdoor air temperature on 18 and 19 January.

Figure 6 shows the numerical and experimental temperatures of the absorber plate and the outlet of DFSC. The temperature deviation of the absorber plate is less than 4 °C. The temperature deviation of the outlet air is less than 3 °C during the daytime when the air vents are open. When the air vents were closed, experimental outlet temperature was higher than the numerical results. It is because the vents were blocked by the insulation blocks, and the temperature sensor located at the upper vent was close to the wall when the vent was filled with the block. The temperature obtained by the sensor was the wall temperature rather than the air temperature in this period of time.
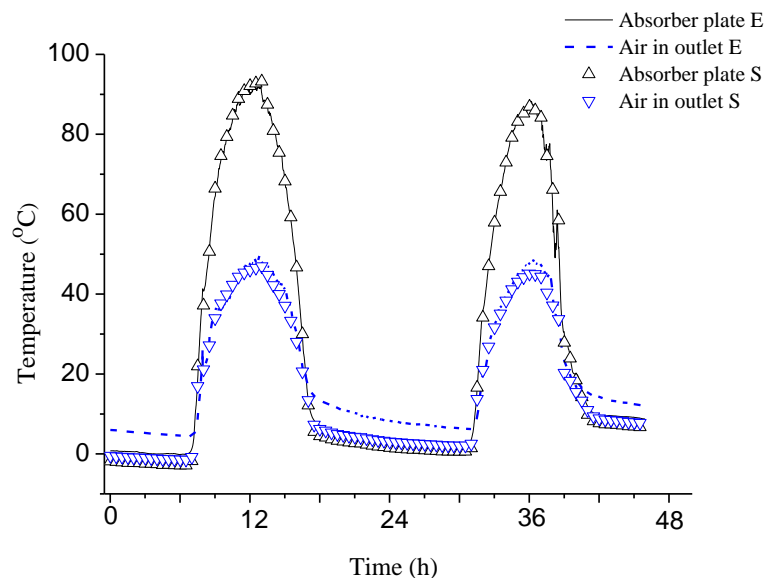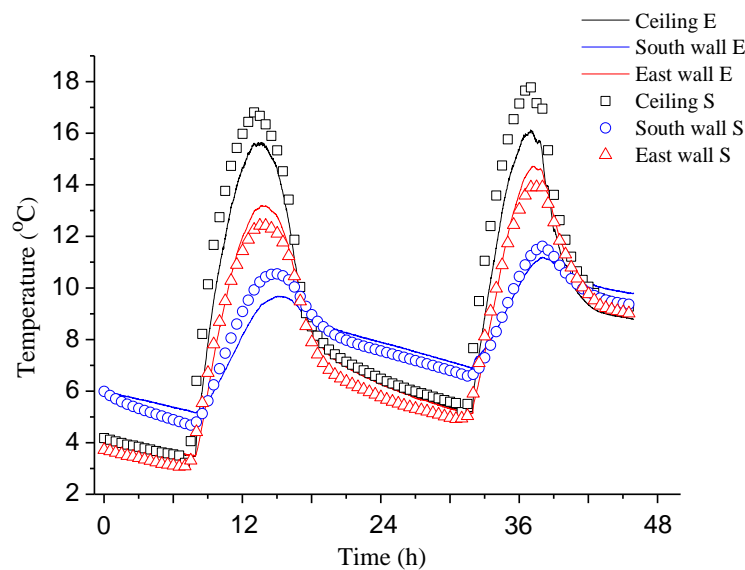

Figure 6. Comparison of measured and predicted temperatures of absorber plate and outlet of DFSC (E—experiment; S—simulation).

The numerical and experimental room temperature is shown in Figure 7. The curves represent the temperatures at three different heights in the room (upper, middle and lower positions). It can be seen that the temperature deviations are less than 2.5 °C.
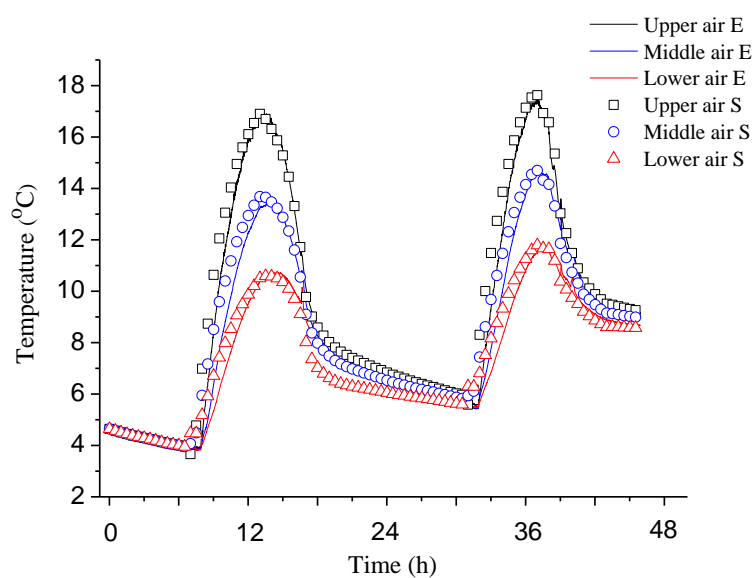
Figure 7. Comparison of measured and predicted temperatures of the indoor air at different height positions (E—experiment; S—simulation).

The model of building involves the walls of four directions, the floor and ceiling. Due to the large heat capacity and the exposed external surface, it is necessary to analyze the heat process of the southern wall. With the exception of the southern wall, the heat transfer processes of other walls with identical materials are the same, so the temperatures of western and northern wall can be represented by the value of the eastern wall. The numerical and experimental results are given in Figure 8. It can be seen that the curves are well matched during the night when the air vents are closed. It is worth mentioning that temperature deviations during the daytime are slightly larger compared to that in the night. This is because air flow in the test room would be more intense when the air vents were opened at the daytime, and the room air leakage through the interface would cause more heat loss in practice. The temperature deviation of the ceiling is less than 2.5 °C and that of both the southern and eastern walls are less than 1.0 °C.

Figure 8. Comparison of measured and predicted temperatures of the building envelope (E—experiment; S—simulation).

The mean deviations of temperature obtained through numerical simulation and experiment are given in Table 3. Based on the above analysis, it can be concluded that the numerical results could make a fairly good prediction of the thermal characteristics of the DFSC, air flow and the building envelop under dynamic outdoor conditions.

Table 3. The mean deviations of temperature obtained through numerical simulation and experiment.

Position	Mean Deviation (°C)
Absorber plate	1.2
Outlet of DFSC	2.6
Indoor air (up/middle/low)	0.4/0.43/0.45
Interior surfaces of envelop (ceiling/south/east)	0.74/0.39/0.46

4.2. Experimental Results

4.2.1. Non-Controlled Condition of Indoor Temperature

The experiment on the DFSC system and reference room has been operated on during 18–19 January. The ambient conditions have been given in Figure 5 in Section 4.1. The maximum global solar radiation on the vertical plane for the two days were 750 W/m^2 and 668 W/m^2. The maximum and minimum ambient temperature on 18 January were 4.0 °C and −3.4 °C, and the corresponding values on 19 January were 10.3 °C and −0.7 °C respectively.

Figure 9 shows the temperature of the test room and outdoor ambient. According to the figure, an obvious temperature gradient existed in daytime when the vents were open. The temperatures of different height positions were uniform when the air vents were closed at night. Analysis of the temperature variation along the height indicates that there was a pronounced increase in the early hours on 18 January. As time went by, an increase of solar intensity enhanced the temperature difference and the peak value of 6.3 °C was reached around 13:00.
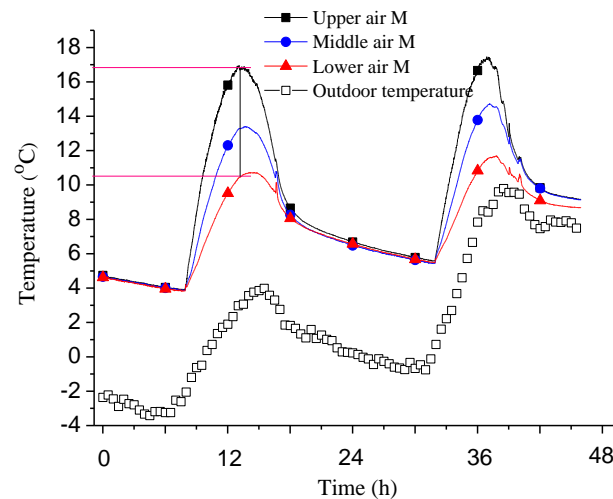
Figure 9. The air temperature distribution of test room and the ambient temperature.

Figure 10 shows the average indoor temperature of the test room and reference room. In general, the temperature of the test room was much higher than the reference room, the effect of DFSC was obvious. The average air temperature of the test room was 8.24 °C, while the reference room was only 4.81 °C, and the test room average temperature was increased by about 3.43 °C after the use of the DFSC. The maximum values of the indoor temperature in the test room and the reference room on the first day were 13.6 °C and 6.3 °C, and the corresponding values on the second day were 14.6 °C and 8.1 °C, respectively. In addition, the maximum temperature of the test room was reached earlier than the reference room. This was because the heat gain of reference room was mainly obtained through the heat conduction of the walls, and the heat gain of test room was transferred not only through the conduction, but also by the air circulation of the DFSC.
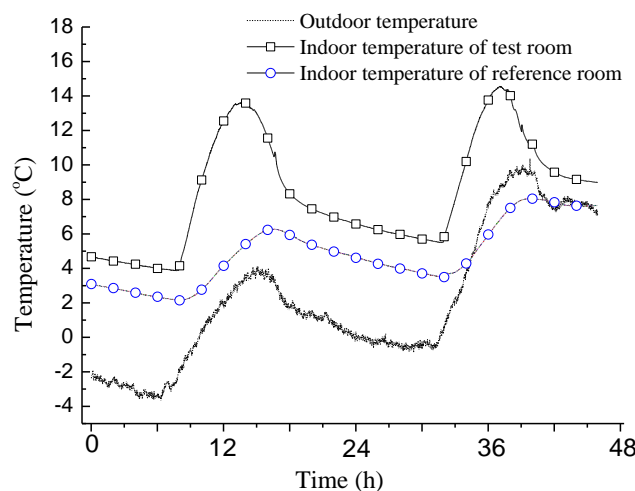
Figure 10. The average temperature of indoor air of the test and reference rooms.

Figure 11 shows heat output of the DFSC. It can be seen that outlet temperature reached up to 51.1 °C and heat output through the collector reached 633.1 W during the experimental period. The inlet temperature has been significantly increased by flowing through the collector under the heated pressure, so the indoor air of the test room can be heated rapidly by the DFSC.
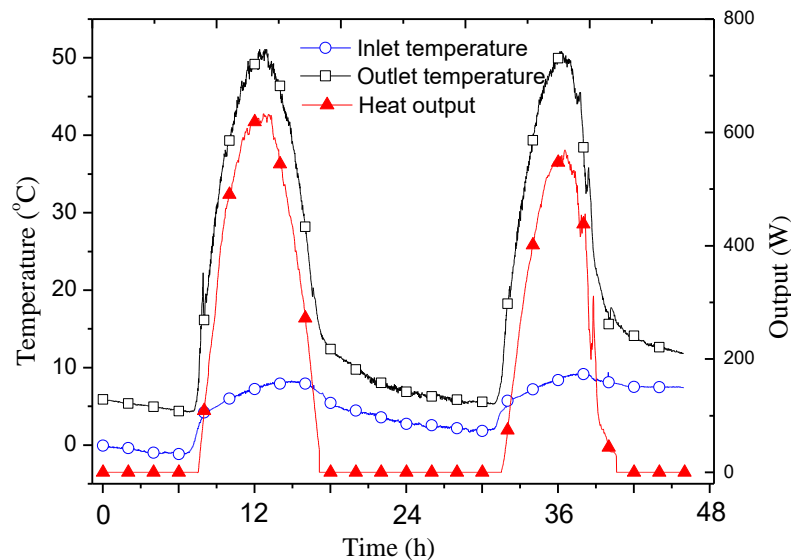

Figure 11. The outlet temperature and heat output of DFSC.

4.2.2. Controlled Condition of Indoor Temperature

In order to evaluate the effect of DFSC on the heating load of building in winter, the temperature control device (electric heating system) was turned on, and the indoor temperature was set to 18 °C. The control strategy of the indoor temperature was: The electric heating device was turned on automatically once the indoor temperature decreased below 18 °C. Otherwise, the electric heating device was turned off if the indoor temperature reached 18 °C. Considering the impact of the heat storage of the walls, the temperature control device was turned on to enable the indoor temperature to reach a steady state at the beginning of the experiment. Figure 12 shows the ambient temperature and the solar radiation during the test time.
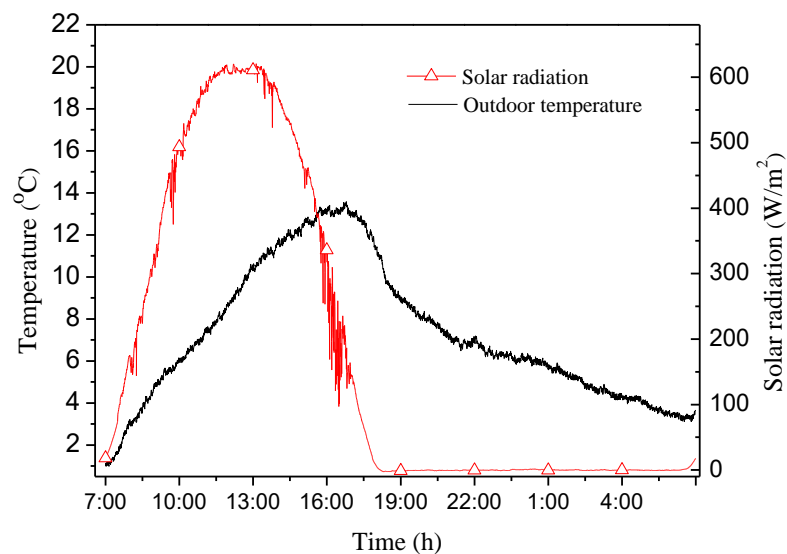

Figure 12. Ambient temperature and solar radiation on 3 March.

Figure 13 shows the electric power consumption of the test room and reference room. In order to keep the room temperature at a constant of 18 °C, both rooms consumed some electricity. However, it can be seen in general that the energy consumed by the test room was less than the reference room. With the ambient temperature and solar irradiance increasing, the electric power consumed by the two rooms decreased while the electric power consumed by the test room decreased faster than reference room due to the DFSC. From 10:30 to 16:30, the electric power consumed by the test room remained at zero, which meant that the test room could maintain the indoor air temperature by the DFSC without needing additional electric power. In contrast, the reference room needed electric heating all the time to maintain a room temperature of 18 °C. As the vents were closed at 17:00, the electric power consumption for the two rooms increased, and the value of both get closer along with time. The experimental results show that the daily power consumption of the test room and reference room are 4.322 kWh and 7.796 kWh, respectively. A power consumption of 3.5 kWh can be saved in a single day. Overall, the winter heating load of building can be significantly reduced by the use of the DFSC operated in passive air heating mode.
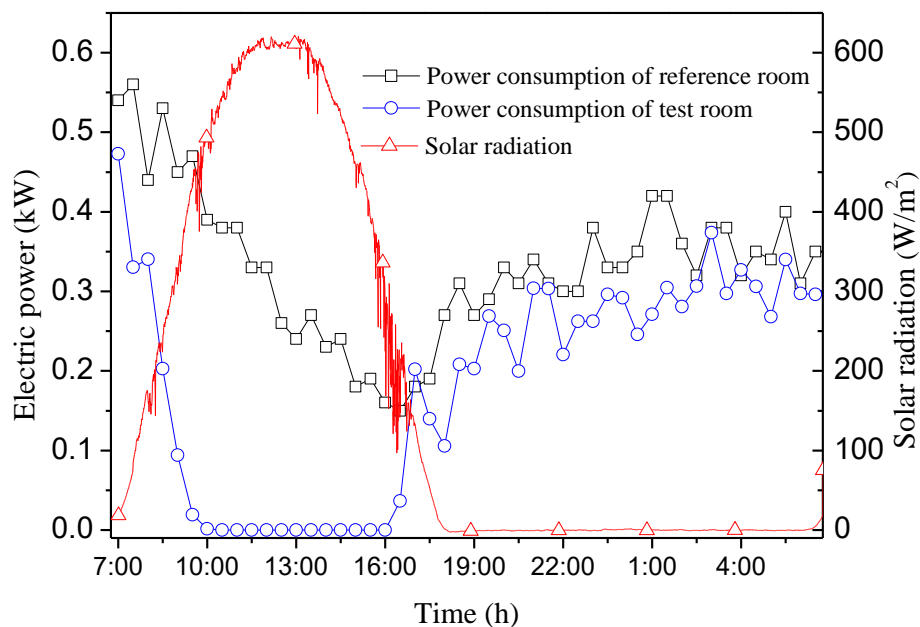

Figure 13. Electric power of test room and reference room.

4.3. Effect of Inner Structure

The numerical simulations are performed to investigate the thermal efficiency of the DFSC and the effect of inner parameters on the efficiency. In the simulation, experimental data on 18 January is used. Figure 14 shows the variation of efficiency from 9:00 a.m. to 5:00 p.m. during the open period of air vents. The highest and lowest efficiency of the DFSC are 47.2% and 33.9%, respectively. The mean daily efficiency is 44.3%.

The structure of Cu-tubes welded on absorber plate aims for the function of water heating. However, few investigations on the effect of the tubes on the passive air heating of the collector have been reported. In what follows, comparisons of a traditional passive solar air collector without the Cu-tubes and the DFSC are made. Figure 15 shows the daily efficiency of the DFSC and traditional passive solar air collector. It can be seen that the efficiency of the DFSC is higher than the traditional passive solar air collector. The tubes increase the heat exchange area of absorber plate, so they act like fins and enhance the heat transfer effect between air flow and absorber plate. The daily efficiency is 44.3% for the DFSC and is 43.6% for the traditional solar air collector.
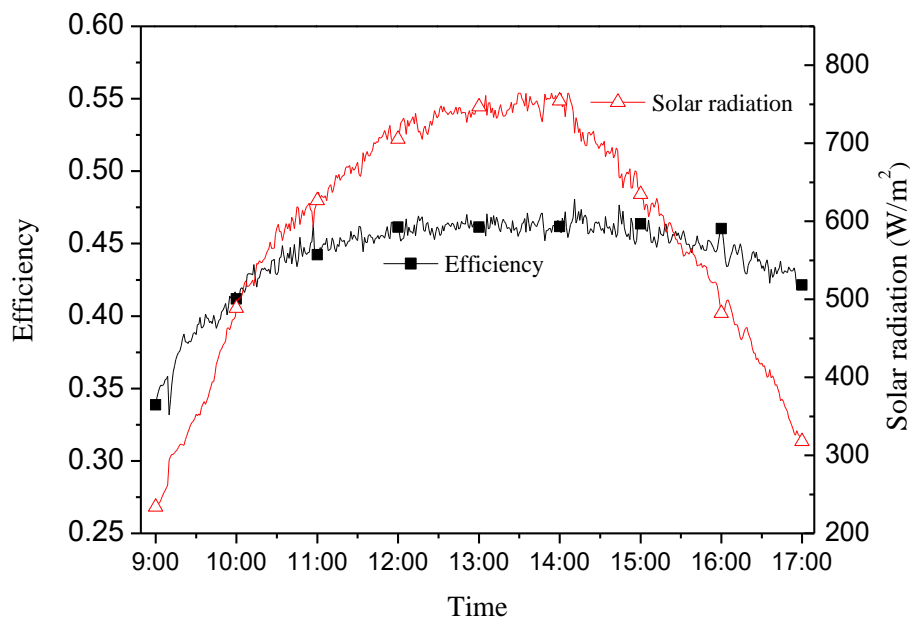
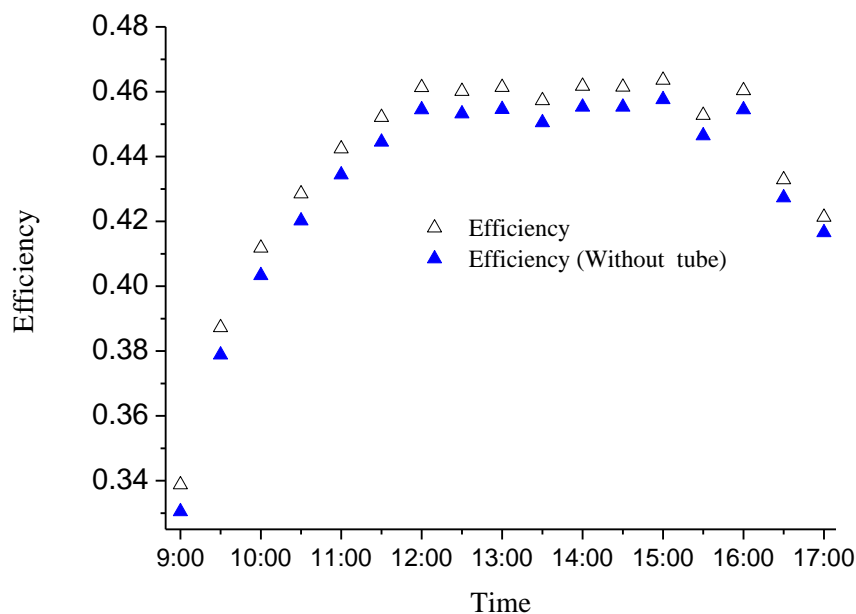**Figure 14.** Efficiency of DFSC and solar radiation.

Figure 15. The daily efficiency of DFSC and traditional passive solar air collector that with no tube.

The effect of the air channel depth on the daily average efficiency of DFSC and the traditional passive solar air collector is shown in Figure 16. It can be seen that either the efficiency of DFSC or traditional solar air collector are increased with the increase of the channel depth. The increase of the thermal efficiency is noticeable until the depth of air channel is greater than 40 mm. Therefore, the depth of air channel is preferably set at 40 mm. In this condition, the structure of Cu-tubes aimed at the function of water heating is beneficial to the thermal performance of passive air heating.

Experiments on the buildings with and without the DFSC were carried out under two conditions: The set-point room temperature of 18 °C, and without a controlled room temperature. Without the control of the room temperature, the average temperature of the test room was 8.24 °C and the reference room was only 4.81 °C. Under the set-point temperature 18 °C, the power consumption of the test room and reference room were 4.322 kWh and 7.796 kWh, respectively.
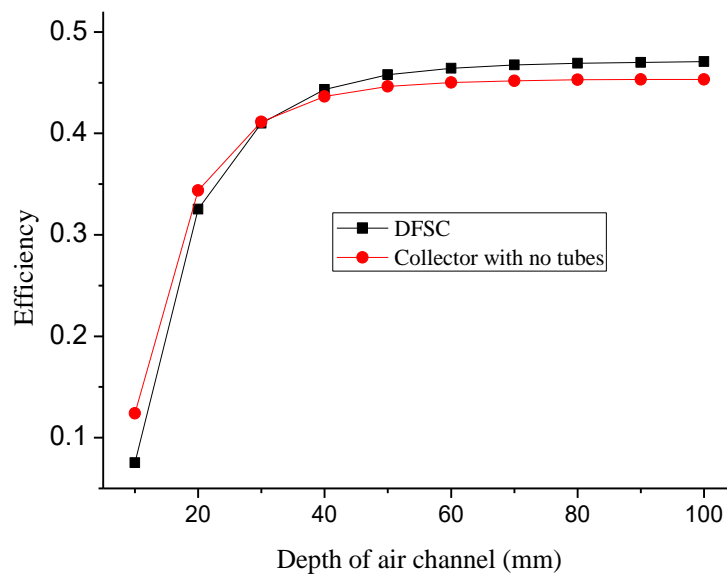
Figure 16. Effect of the air channel depth on the daily average efficiency.

Based on the analysis of Figures 6–8, it can be concluded that the numerical results could make a fairly good prediction of the thermal characteristics of the DFSC, air flow and the building envelop under dynamic outdoor conditions. Adopting the validated model, the impact of Cu-tubes welded on the absorber was analyzed. When the air channel depth is low (less than 30 mm), efficiency of the traditional solar air collector is higher than the DFSC, and Cu-tubes have a negative effect on the performance of passive heating in this situation. When the depth exceeds 30 mm, performance of the DFSC is better than the traditional solar air collector. However, the depth of air channel is preferably set at 40 mm according to the general trend, so Cu-tubes could improve the performance in this condition.

The building-integrated dual-function solar collector is able to provide passive space heating in cold winter, and water heating in warm seasons. In this work, experiments were carried out in three typical days in winter to investigate the thermal behavior of passive heating, which is not enough to study the annual characteristics of the system. In future studies, the performance of DFSC in water heating mode would be investigated and experiments under different conditions would be carried out.

5. Conclusions

The module of a dual-function solar collector (DFSC) was integrated with a building located in Hefei, China. Based on the experimental and numerical study, the following can be concluded:

Comparative experiment showed that room temperature can be increased by about 3.43 °C in winter due to the use of the DFSC.

When the room temperature was set at 18 °C, power consumption of 3.5 kWh could be saved in one day after use of the DFSC.

The numerical results indicated that mean daily thermal efficiency of the DFSC was 44.3%. The efficiency of the DFSC is higher than traditional passive solar air collector that with no water tube. The tubes can increase the heat exchange area of absorber plate. On the other hand, influence of the air channel depth on the thermal efficiency of the DFSC has been analyzed. The results showed that the depth had a prominent effect on efficiency of the DFSC until the corresponding value was greater than 40 mm.

Conflicts of Interest: The authors declare there is no conflict of interest.

Nomenclature

A	area (m^2)
C	specific heat capacity (J/kg K)
d	thickness or depth (m)
De	hydraulic diameter (m)
Gr	Glashov number
hc	convective heat-transfer coefficient (W/m^2 K)
hr	radiative heat-transfer (W/m^2 K)
k	thermal conductivity (W/m k)
L	length (m)
N	numbers of Cu-tubes
P	perimeter (m)
q	heat flux (W)
r	radius of Cu-tubes (m)
S	solar radiation (W/m^2)
t	time (s)
T	temperature (K)
u	velocity (m/s)
v	volume (m^3)
w	width (m)
Greek symbols	
α	absorptivity
β	expansion coefficient
ε	emissivity
η	efficiency
λ	friction loss coefficient
ν	kinematic viscosity (m^2/s)
ρ	density, kg/m^3
τ	transmittance
ξ	partial resistance loss coefficient
Subscripts	
a	air
b	interior plate of backboard
f	air stream
g	front glazing
i	walls in different direction
in	inlet
out	outlet
p	absorbing plate
r	insulation
s	sky
t	Cu-tube
w	wall

References

1. Ma, Q.; Fukuda, H.; Lee, M.; Kobatake, T.; Kuma, Y.; Ozaki, A. Study on the utilization of heat in the mechanically ventilated trombe wall in a house with a central air conditioning and air circulation system. *Appl. Energy* **2018**, *222*, 861–871. [CrossRef]
2. Yu, B.; Jiang, Q.; He, W.; Hu, Z.; Chen, H.; Ji, J.; Xu, G. The performance analysis of a novel TC-Trombe wall system in heating seasons. *Energy Convers. Manag.* **2018**, *164*, 242–261. [CrossRef]
3. Hu, Z.; He, W.; Ji, J.; Zhang, S. A review on the application of Trombe wall system in buildings. *Renew. Sust. Energ. Rev.* **2017**, *70*, 976–987. [CrossRef]
4. Bojić, M.; Johannes, K.; Kuznik, F. Optimizing energy and environmental performance of passive Trombe wall. *Energy Build* **2014**, *70*, 279–286. [CrossRef]
5. Corasaniti, S.; Manni, L.; Russo, F.; Gori, F. Numerical simulation of modified Trombe-Michel Walls with exergy and energy analysis. *Int. Commun. Heat Mass* **2017**, *88*, 269–276. [CrossRef]
6. Imessad, K.; Messaoudene, N.A.; Belhamel, M. Performances of the Barra–Costantini passive heating system under Algerian climate conditions. *Renew. Energy* **2004**, *29*, 357–367. [CrossRef]
7. Sun, W.; Ji, J.; Luo, C.; He, W. Performance of PV-Trombe wall in winter correlated with south façade design. *Appl. Energy* **2011**, *88*, 224–231. [CrossRef]
8. Bellos, E.; Tzivanidis, C.; Zisopoulou, E.; Mitsopoulos, G.; Antonopoulos, K.A. An innovative Trombe wall as a passive heating system for a building in Athens—A comparison with the conventional Trombe wall and the insulated wall. *Energy Build* **2016**, *133*, 754–769. [CrossRef]
9. Briga-Sá, A.; Martins, A.; Boaventura-Cunha, J.; Lanzinha, J.C.; Paiva, A. Energy performance of Trombe walls: Adaptation of iso 13790:2008(e) to the portuguese reality. *Energy Build* **2014**, *74*, 111–119. [CrossRef]
10. Mootz, F.; Bezian, J.J. Numerical study of a ventilated facade panel. *Sol. Energy* **1996**, *57*, 29–36. [CrossRef]
11. Burek, S.; Habeb, A. Air flow and thermal efficiency characteristics in solar chimneys and Trombe walls. *Energy Build* **2007**, *39*, 128–135. [CrossRef]
12. Ghrab-Morcos, N.; Bouden, C.; Franchisseur, R. Overheating caused by passive solar elements in tunis. Effectiveness of some ways to prevent it. *Renew. Energy* **1993**, *3*, 801–811. [CrossRef]
13. Stazi, F.; Mastrucci, A.; Perna, C.D. The behaviour of solar walls in residential buildings with different insulation levels: An experimental and numerical study. *Energy Build* **2012**, *47*, 217–229. [CrossRef]
14. Rockendorf, G.; Janssen, S.; Felten, H. Transparently insulated hybrid wall. *Sol. Energy* **1996**, *58*, 33–38. [CrossRef]
15. Ji, J.; Luo, C.; Chow, T.-T.; Sun, W.; He, W. Thermal characteristics of a building-integrated dual-function solar collector in water heating mode with natural circulation. *Energy* **2011**, *36*, 566–574. [CrossRef]
16. Ji, J.; Luo, C.; Sun, W.; He, W.; Pei, G.; Han, C. A numerical and experimental study of a dual-function solar collector integrated with building in passive space heating mode. *Chin. Sci. Bull.* **2010**, *55*, 1568–1573. [CrossRef]
17. González-González, S.L.; Tejero-González, A.; Rey-Martínez, F.J.; Andrés-Chicote, M. Alternative for summer use of solar air heaters in existing buildings. *Energies* **2017**, *10*, 985. [CrossRef]
18. Shen, J.; Lassue, S.; Zalewski, L.; Huang, D. Numerical study on thermal behavior of classical or composite Trombe solar walls. *Energy Build* **2007**, *39*, 962–974. [CrossRef]
19. Bejan, A. *Convection Heat Transfer*, 4th ed.; John Wiley &Sons: Hoboken, NJ, USA, 2013.
20. Beausoleil-Morrison, I. The Adaptive Coupling of Heat and Air Flow Modelling within Dynamic Whole-Building Simulation. Ph.D. Thesis, University of Strathclyde, Glasgow, UK, 2000.